High energy quantum dynamics of the 15 N + o-14 N 14 N rovibrational activation and isotope exchange processes

Grégoire Guillon, Maxence Lepers, Anuj Tak, Tammineni Rajagopala Rao, Pascal Honvault

High energy quantum dynamics of the ^{15}N + o-^{14}N^{14}N rovibrational activation and isotope exchange processes

Grégoire Guillon,*,† Maxence Lepers,† Anuj Tak,‡ Tammineni Rajagopala Rao,‡ and Pascal Honvault†

†*Laboratoire Interdisciplinaire Carnot de Bourgogne, UMR CNRS 6303, Université de Bourgogne-Franche-Comté 21078 Dijon Cedex, France*

‡*Department of Chemistry, Indian Institute of Technology Patna, Patna 801103, India*

E-mail: gregoire.guillon@u-bourgogne.fr

Abstract

We report full quantum reaction probabilities, computed within the framework of time-independent quantum mechanics using hyperspherical coordinates, for the ^{15}N + ^{14}N^{14}N inelastic and reactive collision processes, restricted to total angular momentum $J = 0$, for kinetic energies up to 4.5 eV. We take advantage of the nonzero ($i = 1$) nuclear spin of ^{14}N, leading to the existence of two nuclear spin isomers of ^{14}N^{14}N, namely ortho- and para-^{14}N^{14}N, to restrict the study to the ortho molecular nitrogen species, with even rotational quantum numbers $j = 0, 2, \ldots$ states. Specifically, we will start with diatomic reagents ortho-^{14}N^{14}N in initial rotational state $j = 0$. A comparison with similar works previously published by other groups using time-dependent wave packet and quasi-classical trajectory methods for the ^{14}N + ^{14}N^{14}N fully symmetric collision is given. We find that reactive processes ^{15}N + ^{14}N^{14}N involving atom

exchange are not happening for collision energies less than 2.2 eV. Collisions at energies around 2.0 eV are most effective for populating reactants rovibrational states, i.e. for inelastic scattering, whereas those at energies close to 5.0 eV yield newly formed $^{14}N^{15}N$ isotopologue in a wide variety of excited vibrational levels.

Introduction

Nitrogen has only two stable isotopes: ^{14}N and ^{15}N, with terrestrial abundances of 99.64% and 0.36%, respectively. As a consequence, it is not as favourable as oxygen (which has three stable isotopes) for the separation between different kinds of isotopic anomalies in fractionation processes, for example those due to nuclear processing within stars and those due to purely chemical effects, in an astrophysical, cosmochemical and atmospheric contexts.[1–6]

Also, the N_2 molecule undergoes predissociation, to give active nitrogen $N(^4S)$ or $N(^2D)$ in the far-UV absorption band, between 80 and 100 nm, generally in the upper part of nitrogen-rich planetary atmospheres. The dissociation yields, starting from the respective species $^{14}N^{14}N$ and $^{15}N^{14}N$, appear somewhat different.[7] The chemistry of the substituted isotopologues of N_2 is thus of great importance, particularly in the hot, upper atmospheres of Earth or Titan.

On the experimental side, some attempts to evaluate rate constants for the title $N + N_2$ exchange process have been made using ^{15}N isotope.[8,9] The $^{15}N^{14}N$ molecule has first been explicitly considered as a test reaction product of $^{14}N + {}^{15}NO \longrightarrow {}^{15}N^{14}N + O$, starting with a sample of pure ^{15}NO. This reaction was used for active atomic nitrogen N titration purposes in various mixtures. As it happens, the explicit $^{15}N + {}^{14}N^{14}N$ exchange process was first investigated as a reaction occurring in this context. Already at that time, this reaction was known to be extremely slow, even for temperatures as high as 1 300 K,[8] with virtually no isotope exchange happening, as stressed also by Lyon,[10] up to 1 200-1 300 K, with a different method. But globally, there exist only few kinetic experimental data[8,10,11] concerning the $N + N_2 \longrightarrow N_2 + N$ exchange reaction.

We can mention another early shock-tube kinetic study[11] of isotope exchange reactions $^{15}N + {}^{14}N{}^{14}N \longrightarrow {}^{15}N{}^{14}N + {}^{14}N$ and $^{14}N + {}^{15}N{}^{15}N \longrightarrow {}^{14}N{}^{15}N + {}^{15}N$ back in 1967, which may occur when oxygen is added to a mixture of $^{14}N{}^{14}N$ and $^{15}N{}^{15}N$, at temperatures up to 3 400 K. One reaction rate for the exchange process has been measured at 3 400 K, with a relatively large error bar.[11] Yet these data are important for the study of high temperature nitrogen plasmas, formed in electric or microwave discharge experiments.[12] Or, even more typically, for the flow-field modeling at high temperatures, including reactive N radicals chemistry, occuring when huge heat load in atmospheric gas results from a shock wave, in the context of heat-shield design for atmospheric high-speed entry of spacecrafts or other space objects where the temperature can reach 20 000 K.[13]

At least three families of potential energy surfaces (PESs) for the ground electronic quartet state ($^4A''$) of the N_3 system, with full permutation symmetry of the nuclei, have been in use for this reaction dynamics. A first empirical LEPS-type PES, with only one adjustable Sato parameter, was built in 1987 by the Perugia (Italy) group.[14] It allows for a dominating colinear minimum energy path (MEP) connecting to the triradical N_3 complex, at the top of a barrier 36 kcal/mol (1.56 eV) high. This first kind of PES has been improved several times, using the LAGROBO (Largest Angle Generalized Rotation Bond Order) procedure based on a dedicated new functional form.[15] This has given the succesive versions of semi-empirical L-PESs, which were named L0 to L3,[16] L4[17] and L4w[18] PESs. This notably led to the transition from a linear to a bent (with around 120° angle) saddle point (transition state), as first suggested by initial tentative ab initio calculations.[19]

Meanwhile and independently, a group attached to NASA Ames Research Center in Moffett Field in California, for spacecraft atmospheric re-entry studies, has produced a new completely ab initio PES in 2003 from more than 3 300 geometries,[20] which again has been used for a variety of dynamical studies[21–23] in subsequent years, named WSHDSP after the authors' names. This full PES stands as a global continuation, based on much more ab initio data, of preliminary $N - N_2$ effective potential interaction calculations, for use in obtaining

transport properties of nitrogen mixtures.[24] This WSHDSP PES presents a MEP, for 119° bent geometry of N_3, with two barriers along (thus two transition states (TS)), of height 47 kcal/mol (2.04 eV), separated by a shallow well deep, called a 'Lake-Eyring' structure.

Finally, a last full dimensional global ab initio PES for the N_3 $^4A''$ ground electronic state, also with three equivalent minima of C_{2v} geometry, has been proposed by the Varandas group in Coimbra.[25] It is based on a mixed set of ab initio data points, from both CCSD(T) and MRCI(+Q) methods, with complete basis set (CBS) extrapolation procedure. It is expressed as a double many-body expansion (DMBE) functional form. It also exhibits a bent 118° MEP, with double barrier height of 45.9 kcal/mol (1.99 eV), and a Lake-Eyring minimum in between at 42.9 kcal/mol (1.86 eV) above atom-diatom dissociation limit, slightly lower than previous computational estimates.[22] We shall refer to this PES as the GV-DMBE PES.

The Perugia LEPS and L-PESs have been used in quasiclassical trajectory (QCT),[14] initial-value representation semiclassical (IVRSC) based on flux-correlation formalism,[26] full dimensional multi-configurational time-dependent Hartree (MCTDH) and time-independent quantum mechanics (TIQM)[18] with the ABC code.[27] These studies were done in particular for gaining understanding of the translation-vibration energy transfer in the $^{14}N + {}^{14}N^{14}N(v) \longrightarrow {}^{14}N^{14}N(v') + {}^{14}N$ process for highly vibrationally excited reactants.[14] On the other hand, the WSHDSP PES has been dedicated to quantum time-dependent wave packet (TDWP) dynamics,[22] with eventual use of J-shifting procedure.[23] In all these studies, collision energies for dynamical observables were often limited to roughly 3.0 eV, and never higher than 4.0 eV. Interestingly, "exact" all-J full-dimensional quantum ICSs and rate constants, based on a completely ab initio PES have never been obtained to date. QCT calculations for the vibrational relaxation and atom exchange processes, have been realized based on the GV-DMBE PES by the same group that has built it,[28] showing a slightly higher reactivity than revealed by previous, above mentioned studies. It is the latter PES - the GV-DMBE PES, from the authors' names - that we shall use in our present dynamics study.

Now, in spite of the existence of experimental measurements of concentrations of heavy

isotope substituted nitrogen molecules $^{14}N^{15}N$ in the atmosphere,[6] and despite explicit use of ^{15}N isotope in kinetic experiments,[10] the authors are not aware of a systematic theoretical study of the $^{15}N + {}^{14}N^{14}N \longrightarrow {}^{15}N^{14}N + {}^{14}N$ reactive process.

In the present study, we shall look at collisions involving only one ^{15}N atom, and focus on the reactive process, not studied so far:

$$^{15}N(^4S_u) \; + \; ^{14}N^{14}N(^1\Sigma_g^+) \; \longrightarrow \; ^{15}N^{14}N(^1\Sigma_g^+) \; + \; ^{14}N(^4S_u)$$

We will abreviate it as $5 + 44 \longrightarrow 54 + 4$. This isotopic process has the advantage of eliminating the quantum ambiguity inherent to the use of three identical nuclei ^{14}N. Due to the low abundance of ^{15}N in Earth atmosphere (3.67×10^{-3} times lower than for ^{14}N), we shall not expect this reaction to happen significantly in the whole atmosphere, but it may be important in the upper part. Also, as mentioned above at length, a study involving the $^{15}N^{14}N$ molecule presents several interests. With a view to high-temperature applications, we decided to run calculations for collision energies as high as 4.5 eV. For integral cross sections properly obtained up to this energy, this should yield converged rate constants for temperatures up to 10 000 K.

As explained in the Appendix Section, two nuclear spin isomers of molecular nitrogen coexist, namely ortho ($o-^{14}N^{14}N$) and para ($p-^{14}N^{14}N$) forms of N_2, thereafter called as o44 and p44, which are susceptible to bring different resonance structures in the reaction probabilities, or cross sections if all J computations are performed. In the present paper, we consider the reactive process mentioned above, as well as the rovibrational excitation induced by inelastic collision, starting from o44 as a reagent diatomic molecule, restricted to zero total angular momentum ($J = 0$).

As numerous results were already presented starting from excited initial vibrational and rotational states, for the $^{14}N + {}^{14}N^{14}N$ reaction, based on various PESs,[14,18,21–23,28] we have chosen instead to focus on vibrational state-to-state transitions toward a variety of excited

vibrational levels v', among which we present the most significant and illustrative results.

Theory, modeling and computations

The process under consideration is realized at relatively high collision energy. Therefore, the only aspect in this work where nitrogen nuclear spin intervenes is in the nuclear spin-states statistics. The Hamiltonian is devoid of any nuclear spin-dependent components.

Our present collision system, 5 + 44, is of $A + X_2$ type, with two possible arrangements. It exhibits two identical nuclei ^{14}N with spin $i = 1$ in the diatomic molecule ^{14}N^{14}N (44) in the entrance channel. The ^{15}N nuclear spin, $i = 1/2$, is not of interest for us in this study. We thus have to separate between the two existing nuclear spin isomers, namely para-^{14}N^{14}N, written p44 (with odd rotational states $j = 1, 3, \ldots$) and ortho-^{14}N^{14}N, or o44 (with even rotational states $j = 0, 2, \ldots$), from the begining, in treating the dynamics and calculating the scattering and reaction probabilities (SPs and RPs). After that, we need to compute spin isomer statistical weights of each symmetry (*i.e.* ortho and para) from an enumeration of the allowed nuclear spin functions.

Finally, SPs and RPs resulting from our calculations and belonging to the appropriate symmetry (of the $\mathcal{S}_2$ permutation group), when compared to that of the spin function, in accordance with the Pauli principle for the global electro-nuclear wavefunction, will be multiplied by the corresponding spin-weights. All the details are explained in the Appendix Section.

On the numerical side, we have performed TIQM scattering calculations to extract SPs and RPs at total angular momentum $J = 0$, for both the 5 + o44 inelastic activation, and reactive (with atom exchange), collisions, at high kinetic energies ranging between 1.90 and 4.50 eV. The dynamical calculations are supported by a formerly developed potential energy surface, from the Galvão and Varandas group,[25] the so-called GV-DMBE PES mentioned in the Introduction Section. The GV-DMBE PES has already been used by the same group[28]

and has proved to be accurate for scattering purposes, as found with QCT dynamics studies of the $^{14}N + {}^{14}N^{14}N$ collision.[28]

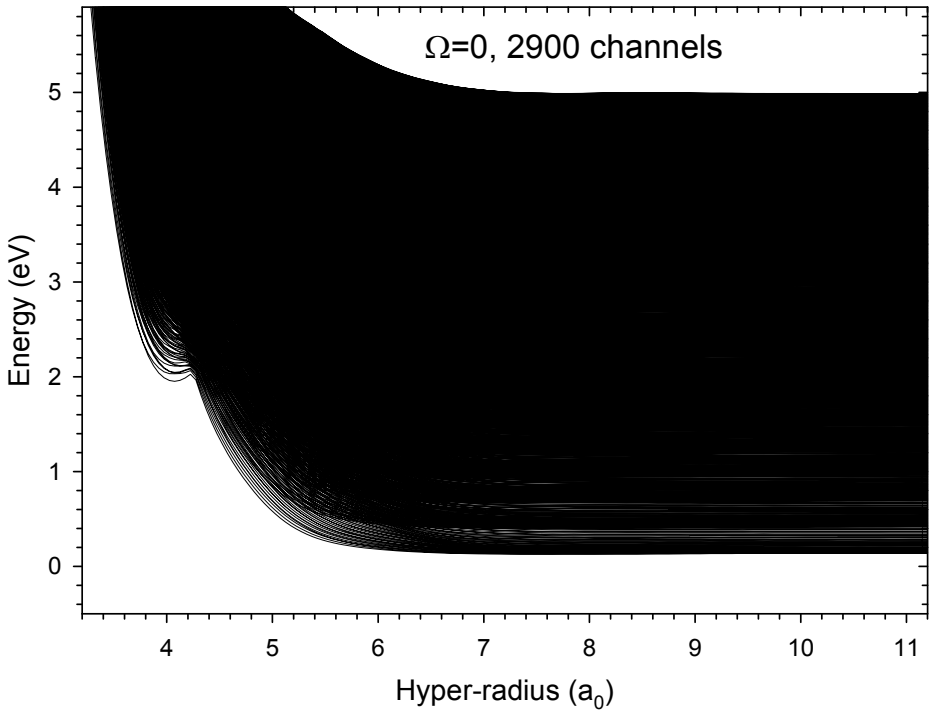

Figure 1: The whole of 2900 adiabatic energies (or adiabats), in eV, for the $^{15}N^{14}N^{14}N$ system, with $\Omega = J = 0$, as a function of the hyper-radial coordinate ρ, between 3.2 and 11.2 a_0. The adiabat density is extremely high, with highest channels reaching 5.0 eV asymptotically.

To obtain these observables, we have solved "exact" close-coupled equations (in the hyper-radial functions $F^{JME}_{k\Omega;\lambda vjl}(\rho_m;\rho)$, see below for the details of notation) arising from the nuclear, time-independent, Schrödinger equation (TISE) expressed in principal axis body-fixed democratic hyperspherical coordinates. The method has already been described in detail in the theoretical reference,[29] and has already been successfully employed, notably for the $O + O_2$ collision.[30–34] Accordingly, we shall only mention the coordinates and the specific calculation parameters we have used in this study.

The Delves-Fock hyperspherical coordinates[35] may be defined from mass-scaled Jacobi

coordinates:

$$\rho \equiv \sqrt{\mathbf{s}_\lambda^2 + \mathbf{S}_\lambda^2}$$

$$\omega_\lambda \equiv \arctan \frac{s_\lambda}{S_\lambda}$$

where $s_\lambda \equiv |\mathbf{s}_\lambda|$ et $S_\lambda \equiv |\mathbf{S}_\lambda|$, and

$$(\mathbf{s}_\lambda, \mathbf{S}_\lambda) = (d_\lambda^{-1}\mathbf{r}_\lambda, d_\lambda \mathbf{R}_\lambda)$$

with $(\mathbf{r}_\lambda, \mathbf{R}_\lambda)$ usual Jacobi coordinates and d_λ the mass-scale factor.[29,36] The hyper-radius ρ does not depend on the specific arrangement, while the hyper-angle ω_λ, related to the shape of the three-nuclei triangle, depends on the arrangement λ. The four remaining angles are spherical angles associated with Jacobi vectors: $(\theta_{s_\lambda}\phi_{s_\lambda})$ and $(\theta_{S_\lambda}\phi_{S_\lambda})$.

On the other hand, the least inertia axis, body-fixed democratic hyperspherical coordinates, related to the so-called Smith-Whitten coordinates,[36,37] are defined as:

$$\rho \equiv \sqrt{q^2 + Q^2}$$

$$\theta \equiv \arctan \frac{q}{Q}$$

$$\phi \equiv \frac{1}{2} \arctan \frac{2\mathbf{S}_\alpha.\mathbf{s}_\alpha}{S_\alpha^2 - s_\alpha^2}$$

in which the hyper-radius ρ is redefined in terms of $q \equiv |\mathbf{q}|$ and $Q \equiv |\mathbf{Q}|$, taking the initial arrangement $\lambda = \alpha$ as a reference, and where the two orthogonal vectors $\mathbf{q}$ and $\mathbf{Q}$ are related to $\mathbf{s}_\lambda, \mathbf{S}_\lambda$ by the kinematic transformation[36] $T(\phi_\lambda)$:

$$(\mathbf{q}, \mathbf{Q}) = (\mathbf{s}_\lambda, \mathbf{S}_\lambda) T(\phi_\lambda)$$

By working in body-fixed system and orienting the moving frame along least inertia axis, not only the number of dynamical degrees of freedom is reduced from six to three (6D to

3D), but also the arrangement dependence is lost and the coordinates are called democratic. The three-body hamiltonian, in these coordinates, is expressed as:

$$H = \frac{1}{2\mu}\left[\frac{1}{\rho^5}\frac{\partial}{\partial\rho}\rho^5\frac{\partial}{\partial\rho} - \frac{\Lambda^2(\theta,\phi)}{\rho^2}\right] + V(\rho,\theta,\phi)$$

where $\Lambda^2(\theta,\phi)$ is the square of grand angular momentum operator, including internal hamiltonian operator and Coriolis coupling term, μ is the symmetrized rediced mass, and V the potential.

For a given fixed value of the hyper-radius, $\rho = \rho_0$, common eigenfunctions of operators J_z^2 and H_i (the previously mentioned internal hamiltonian) are, dropping out the reference to ρ_0 for lighter notation:

$$\Phi_{k\Omega}^{JME}(\theta,\phi,\alpha\beta\gamma) = \varphi_{k\Omega}(\theta,\phi)N_{\Omega}^{JM}(\alpha\beta\gamma)$$

with

$$J_z^2\Phi_{k\Omega}^{JME}(\theta,\phi,\alpha\beta\gamma) = \Omega^2\Phi_{k\Omega}^{JME}(\theta,\phi,\alpha\beta\gamma)$$

and

$$H_\Omega\varphi_{k\Omega}(\theta,\phi) = \epsilon_{k\Omega}\varphi_{k\Omega}(\theta,\phi)$$

This quantity is the surface hamiltonian. In these expressions, $(\alpha\beta\gamma)$ triplet is usual Euler angles, which describe the body-fixed orientation, E is the total energy, M is the J-projection on the space-fixed z-axis, and Ω its projection on the body-fixed least inertia axis. The functions N_Ω^{JM} are Wigner's, but with definite parity. The hamiltonian H_Ω is a reduced one, simply defined by replacing J_z^2 operator with its eigenvalue Ω^2 in H_i. Eigenstates $\varphi_{k\Omega}$ and eigenvalues $\epsilon_{k\Omega}$ (the latter being, as a function of ρ, the adiabatic energies represented in Figs. 1 and 2), where k indexes the channel, are obtained from diagonalization of the reduced hamiltonian H_Ω, constructed on the basis of hyperspherical pseudo-harmonics $\mathcal{K}_{K\nu}^{\Omega}$ that obey the generalized eigenvalue equation (in $K(K+4)$ for the 6D Laplacian) for squared

angular momentum in the 5D-hypersphere case.[37]

From a numerical point of view, in this sector-diabatic scheme, the range of the hyper-radial coordinate ρ is divided into 110 small sectors, in which the total wavefunction is expanded on the basis defined at the sector mid-point. The expansion coefficients, functions of ρ, are solutions of a set of coupled hyper-radial equations. These have been numerically solved using the log-derivative propagator.[38,39]

The 5 + 44 process presents a high energy threshold for genuine chemical rearrangement, allowing for the transfer of ^{15}N atom, at around 2.0 eV. Therefore the dynamics of this process becomes interesting starting from the relatively high collision energy $E_c = 1.90$ eV. To be useful in high temperature (up to $T = 10\,000$ K) applications described in the Introduction Section, the collision process has to be simulated at kinetic energies up to $E_c = 4.50$ eV. We note at this point that ab initio calculations have shown the existence of a D_{3h} minimum, 147 kcal/mol (6.4 eV) above the asymptote, resulting from a conical intersection seam between the ground and first excited state of $^4A''$ symmetry. So multi-surface dynamics would be needed for collision energies higher than 5.0 eV.

We have thus decided that, to obtain results in a reasonable time at such high collision energies, calculations should be restricted to $\Omega = 0$ (which is the maximum value of the projection of the total angular momentum J on the least inertia axis of the $^{15}N^{14}N^{14}N$ or 544 complex). Then, for total angular momentum $J = 0$, the solution of the TISE is expanded in the middle of each sector, ρ_m, as:

$$\Psi^{JME}_{\lambda vjl}(\rho;\theta,\phi,\alpha\beta\gamma) = \rho^{-5/2}\sum_{k\Omega}\Phi^{JME}_{k\Omega}(\rho_m;\theta,\phi,\alpha\beta\gamma)F^{JME}_{k\Omega;\lambda vjl}(\rho_m;\rho)$$

in terms of adiabatic surface states previously described and obtained, and, computationally, stored on disk.

In order to be able to obtain converged SPs and RPs at $E_c = 4.50$ eV, we have included as many as 2900 adiabatic states, or "adiabats", at $\Omega = 0$. Their energies, represented as a

function of the hyper-radial coordinate ρ, are shown in Fig. 1. We clearly see the very high density of these states, appearing nearly uniform. At large ρ values, i.e. $\rho \approx 11\ a_0$, they sediment slightly above 5.0 eV, which allow for the entry of many closed channels in the coupled-equations. The unusual hump for the lowest adiabats at around 4.3 a_0 results from the peculiar topography of the GV-DMBE PES, exhibiting a huge volcano-like structure with a crater on top. This outcrop imprints its shape on them.

A close-up is shown in Fig. 2, revealing the very neat ordering of the adiabats, as well as the regular variations in their density, owing to to the appearance of new rotational sub-structure with each new vibrational state.

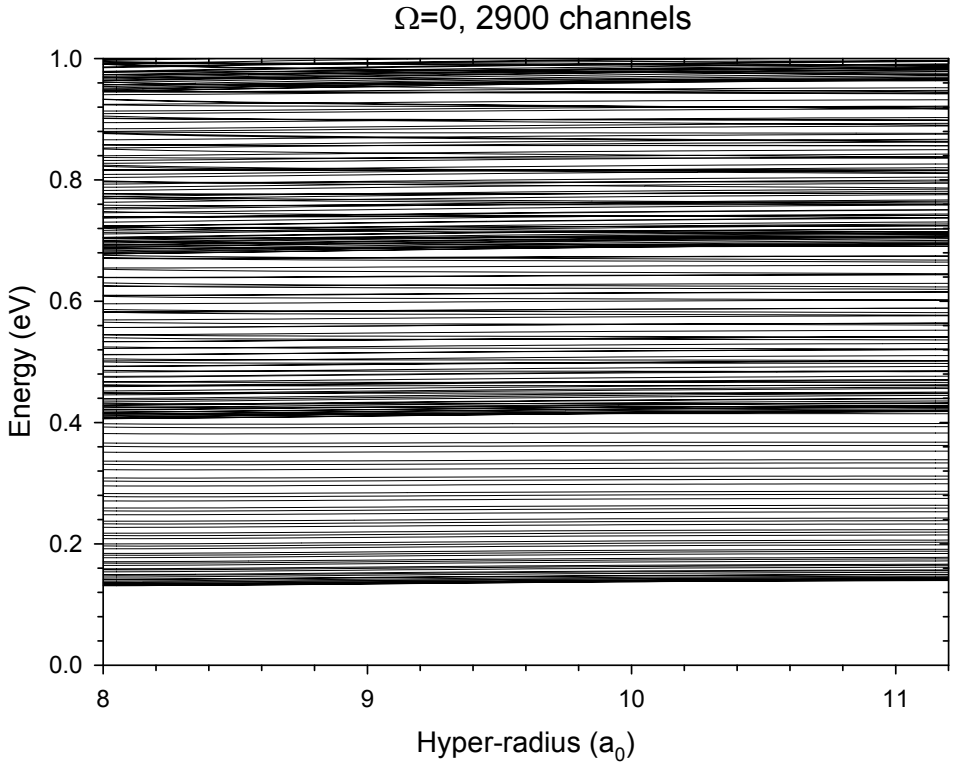

Figure 2: A close-up for the lowest adiabatic energies (or adiabats), below 1 eV, for the $^{15}N^{14}N^{14}N$ system, with $\Omega = J = 0$, as a function of hyper-radial coordinate ρ, between 8.0 and 11.2 a_0. The regular variation in density due to the appearance of new rotational sub-structure with each new vibrational level is clearly visible.

Asymptotically, for each arrangement, the surface states converge to (properly sym-

metrized) rovibrational wavefunctions of Fock internal coordinates,[40] with fragmentation quantum numbers v, j characterizing each channel for matching with the internal region. Due to the high number of channels included at $J = 0$, great care has been taken, especially with regards to two-dimensional quadratures in Fock coordinates, to accurately compute the projections of the total wavefunction onto these asymptotic rovibrational functions re-expressed in space-fixed coordinates. All projections have been obtained within 1% accuracy, and 21 vibrational v numbers, as well as 80 and 159 diatom rotational j numbers have been included, for arrangements 5 + 44 and 4 + 54, respectively, in the basis.

Finally, the reactance $\mathcal{K}$ and transition $\mathcal{T}$ matrices are obtained for a large value of the hyper-radius by matching the propagated solution to its asymptotic form, respecting the boundary conditions for the scattering problem. Numerical tests at these high collision energies have shown that a value $\rho_{\max} = 11.5\ a_0$ was sufficient for our purposes. We have obtained $\mathcal{K}$ matrices at 2 340 energy grid points ranging between 1.90 and 4.50 eV at total angular momentum of $J_{\max} = J = 0$. The SPs and RPs, noted respectively $P^{J\Omega}$ and $N^{J\Omega}$, and this in our case P^{00} and N^{00}, are obtained by direct summation of the squared $\mathcal{T}$-matrix elements.

The sector-by-sector construction of the surface-functions basis took a total of nearly 1 100 hours of CPU time, while each sector basis computation required at most 95 GB of RAM. The overall subsequent building of the complete $\mathcal{K}$-matrix for the whole energy range accumulated around 5 000 hours of CPU time. The whole project amounts to nearly nine months of intensive calculations, on high performance computations (HPC) resources of the local computing center (DNUM CCUB, University of Burgundy in Dijon).

Results and discussion

In this section, we present the initial-state-selected scattering probabilities, for the 5 + o44($j = 0$) inelastic (i.e., without any ^{15}N atom exchange) and reactive (i.e., including ^{15}N

atom exchange) collision processes. These transitions are toward all accessible outcomes energetically open using the TIQM method, allowing a manifold of final vibrational states v', while the reagents remain in the ground vibrational level $v = 0$ within the whole study. By the same token, we will consider in the present paper only collisions starting from the $j = 0$ level of o44. A future study will be dedicated to the 5 + p44($j = 1$) collision.

Initial-state-selected SP and RP

Fig. 3 shows the initial-state-selected scattering probability $P^{00}_{v=0,j=0}(E_c)$ for inelastic activation of o-^{14}N^{14}N in its ground rovibrational state $v = 0, j = 0$ by ^{15}N, i.e. 5 + o44($v = 0, j = 0$) $\longrightarrow$ 5 + o44(all v', all j' even $\neq$ (0,0)) as a function of the collision energy.

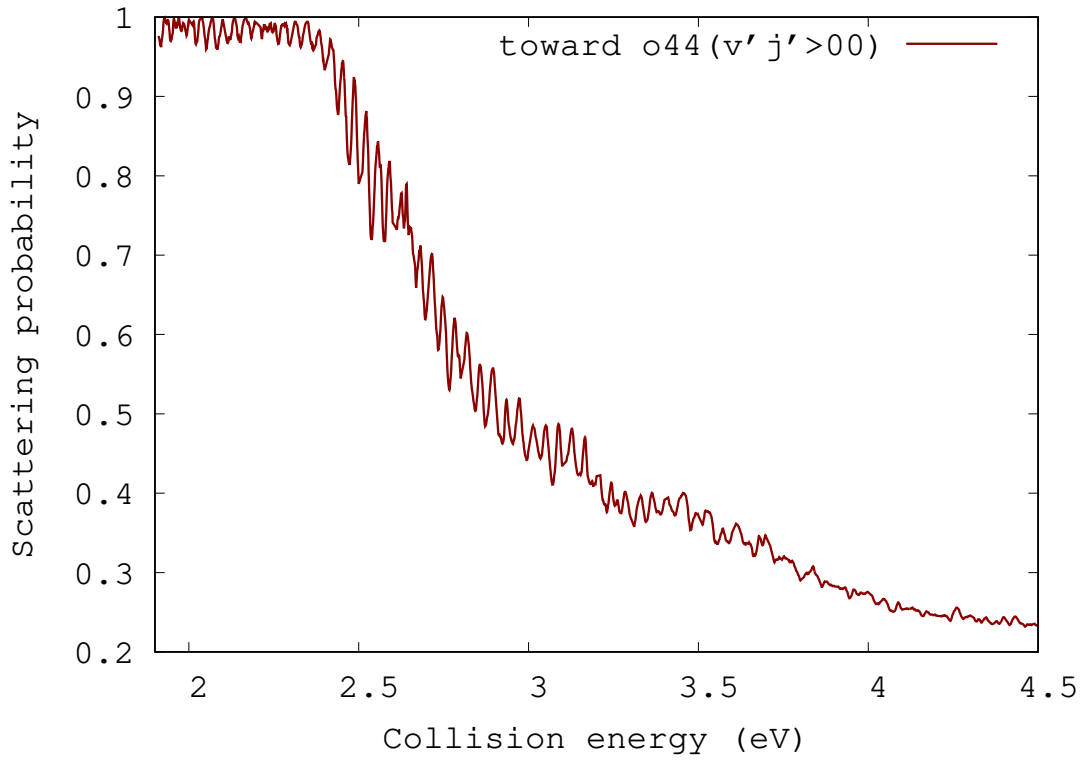

Figure 3: Initial-state-selected scattering probability for inelastic activation of o-^{14}N^{14}N in the ground rovibrational state by ^{15}N in the 5 + o44($v = 0, j = 0$) $\rightarrow$ 5 + o44(all v', all j' even $\neq (0, 0)$) process, as a function of collision energy in eV.

A primary feature in Fig. 3 is that collisions follow a globally monotonic decreasing pat-

tern. We observe a first extremely high plateau at the lowest collision energies, between 1.9 and 2.3 eV, with well marked oscillation structures, the probability of rovibrational activation of o-^{14}N^{14}N reaching unity at regular intervals. Then, a gentle fall happens, starting at roughly 2.4 eV. This onset for the decreasing of the SP with collision energy coincides with the opening of the lowest reactive channels, as can be verified with the corresponding onset, at the same energy, for increasing behavior seen in Fig. 4 (giving the RP as a function of collision energy), redirecting the scattering flux from inelastic collision to genuine reaction. The oscillations during the beginning of the descent are exacerbated, until reaching nearly 0.2 units of amplitude. The global fall continues until 4.5 eV of collision energy, while oscillations are gradually attenuated and begin to fade away. Between 3.7 and 4.5 eV oscillating structures are nearly lost, giving way to a kind of background noise, closer and closer to what looks like a high-energy asymptote value of 0.2. That is, the SP falls down until reaching a threshold. The reason seems to be related to a saturation phenomenon. Indeed, whatever the energy injected to the system, inelastic scattering never vanishes but stabilizes at a background value coming from the addition of higher and higher rovibrational channels of the same arrangement. This can be seen clearly, making an anticipated reference, with the behavior shown in Fig. 5, and described in the next subsection. Excitation probabilities of lowest inelastic channels seem to decrease in amplitude; while this effect is compensated by regular opening of higher and higher (v', j') channels, each contributing only a tiny value to the probability, as E_c increases. The constant background effect comes from the averaging of these numerous small noise values. We see this way that inelastic rovibrational activation processes, without any reactivity, still significantly occur at very high temperatures.

Fig. 4 shows the initial-state-selected genuine $J = 0$ reaction probability, $N^{00}_{v=0,j=0}(E_c)$, for the collision of ^{15}N with o-^{14}N^{14}N in its ground rovibrational state $v = 0, j = 0$, i.e. 5 + o44$(v = 0, j = 0) \longrightarrow 4 + 54$(all v', all j') process, again as a function of the collision energy.

We see right away in Fig. 4 that the RP follows this time a globally monotonic increasing

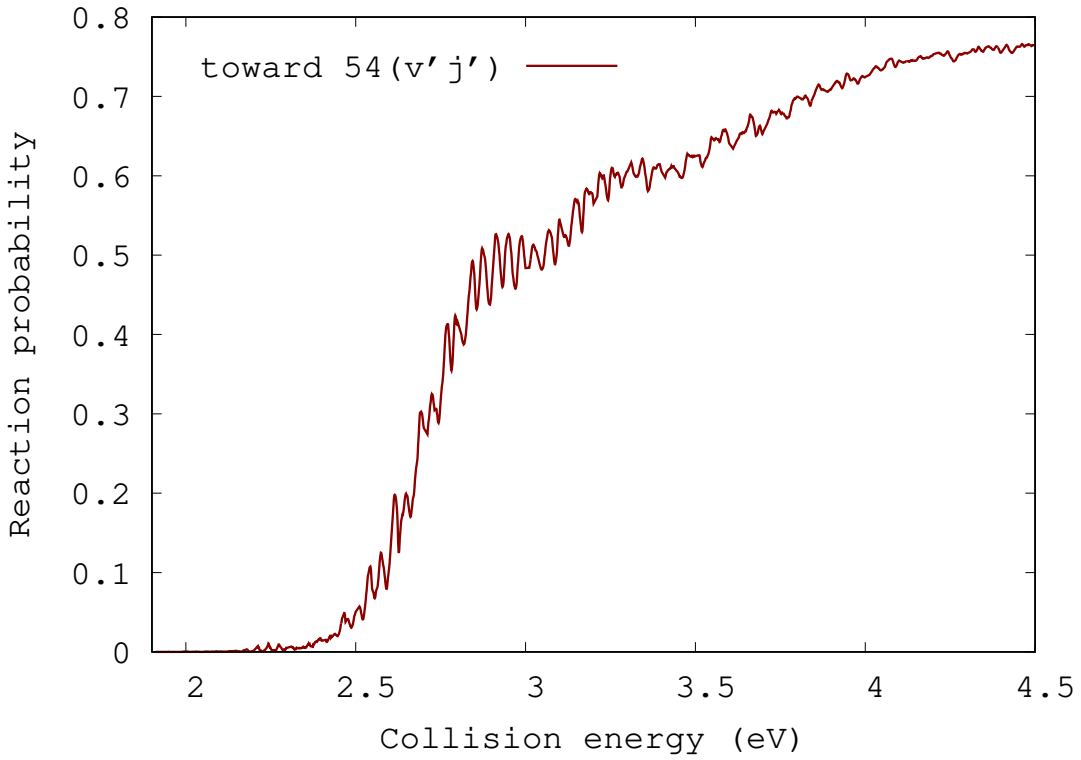

Figure 4: Initial-state-selected reaction probability for atom transfer process of ^{15}N in o-^{14}N^{14}N in its ground rovibrational state: the $5 + o44(v = 0, j = 0) \rightarrow 4 + 54$(all v', all j') process, as a function of collision energy in eV.

pattern, opposite and complementary, as can be expected, to the SP of the inelastic process described above. First of all, the RP remains at zero up to 2.2 eV. Extremely slight oscillations appear for higher energies, the RP dropping to zero again on a regular basis, between 2.2 and 2.3 eV. It starts to take off from 2.3 eV, its shape taking on the appearance of an exponential increase. In this regime, oscillations are strong and clearly visible. We can see it as a kind of transition from the inelastic-dominating process to the reactive atom exchange process. This energy regime terminates with a massif of resonances slightly under 3 eV, where the global tendency of the curve is also changing. The exponential rise breaks off and the RP seems to hesitate between a stabilization plateau or another definite increase. As it happens, the RP actually keeps increasing, while oscillations attenuate, toward a value of 0.77, at 4.5 eV of collision energy, the asymptote being probably reached around 5 eV. Noteworthly, this is in contrast to the behavior obtained by Wang et al.,[21,22] in

TDWP with the WSHDSP PES, where they find a slight decrease of this quantity at around 2.7-2.8 eV. The discrepancy is most probably due to the slight difference in the topography of the Lake-Eyring structure at the top of the outcrop, between the GV-DMBE PES (3.0 kcal/mol deep) and the WSHDSP PES (3.5 kcal/mol deep). All the resonances (which are in fact transparencies) have been shown to be due to the Lake-Eyring feature.[21,22] The shallower minimum associated with the GV-DMBE PES, with thinner double-barrier width, permits more effective tunneling, allowing resonances to build up on each other, yielding a global monotonic increasing behavior. The reactive regime, as compared to the inelastic one, clearly dominates at energies above, let's say, 3.5 eV. We also note that the probability for the reaction 5 + o44 is very structured, with the presence of sharp peaks and troughs that may be associated with Feshbach resonances. These features are signatures of the peculiar "Lake-Eyring" structure at the top of the outcrop on the reaction path, and have been discussed in details by the Moffett Field group.[23] They illustrate tunelling regime in the double barrier case, as we can find in flux-correlation perfected transition state theories.[41] They have actually dedicated a study[21] to the assignement of specific resonances appearing, especially at the lowest collision energies for which reaction occurs, but for the 4 + 44 reaction. In brief, many marked resonances survive the summation process over all final states, in obtaining the initial-state-selected reaction probability, toward all energetically allowed outcome channels.

State-to-state SPs and RPs

In order to gain additional insight into the scattering process, and to further analyse the "low" and "high" energy regime as well as the occuring resonances, we show, in Fig. 5, some illustrative vibrational state-to-state SPs (STS-SPs) at collision energies in the dominating inelastic domain, $E_c \in [1.90, 2.40]$ eV; and in Fig. 6 vibrational state-to-state RPs (STS-RPs) in the reactive regime energy region, $E_c \in [4.00, 4.50]$ eV. These are noted $P^{00}_{(v=0,j=0)\to v'}(E_c)$ and $N^{00}_{(v=0,j=0)\to v'}(E_c)$, respectively. We have chosen these two specific energy intervals be-

cause some previous studies[18,22,23,28] have already focused on the dependance, upon initial and final (v, j) states, of thresholds for RPs in reactive N + N_2 scattering, at E_c starting from 2.0 eV, with strong emphasis on the role of the initial state. We have thus decided to focus in this study on final vibrational states. Also, for high energies, a vibrational state analysis is more relevant than one focusing on rotational states. The vibrational STS-SPs and STS-RPs presented here are summed over all final rotational states j'. At the highest collision energies, o-^{14}N^{14}N rotational excitation reaches states up to $j' = 136$, whereas bond-breacking reaction formed ^{14}N^{15}N populates rotational levels as high as $j' = 138$. We do not show rotationally resolved STS-SPs and STS-RPs here, but instead concentrate on products vibrational state analysis.

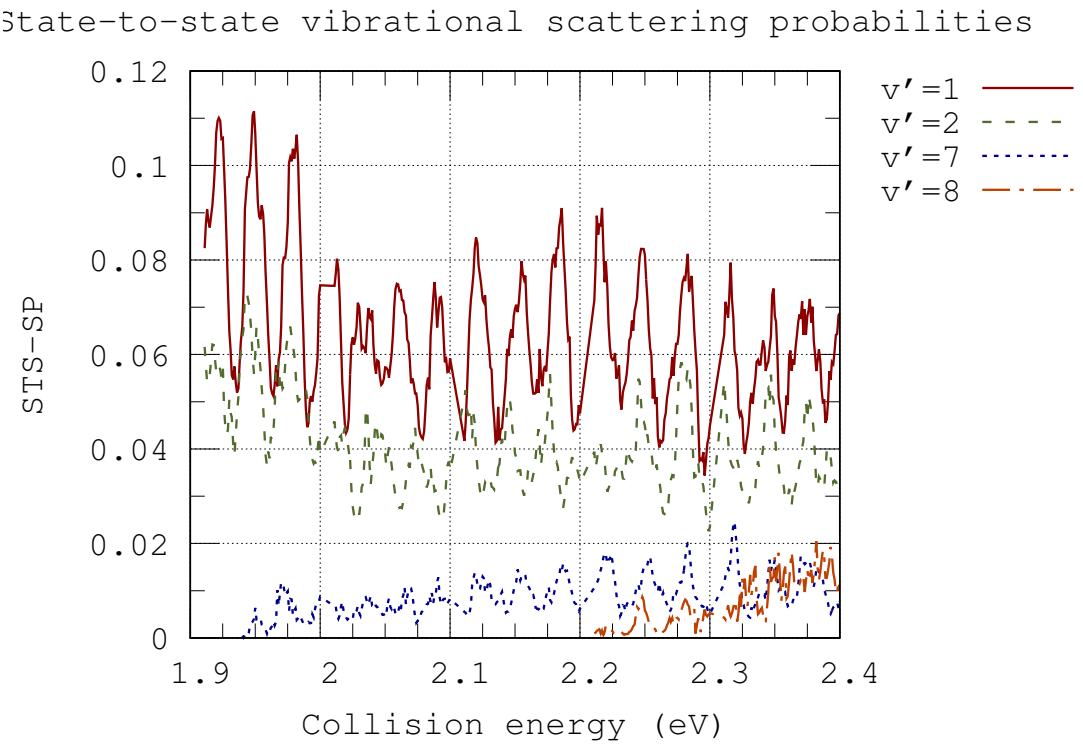

Figure 5: Vibrational state-to-state resolved scattering probabilities for inelastic activation processes of o-^{14}N^{14}N in its ground rovibrational state by ^{15}N: the 5 + o44$(v = 0, j = 0) \rightarrow$ 5 + o44(v', all j' even $\neq (0, 0)$) processes, as a function of collision energy in eV.

We clearly see in Fig. 5 that inelastic activation of o44 to the nearest $v' = 1$-level is the largest one, and exhibits the wildest oscillations on either side of a roughly constant

value. It contributes mostly to the high magnitude oscillating initial-state-selected averaged SP shown in Fig. 3 and previously discussed. The SP for excitation toward the $v' = 2$-level presents a similar behavior, with a lower absolute mean value and amplitude. The SPs for other v' decrease as v' increases and have a similar oscillating behavior, and therefore are not shown. Finally, we show SPs toward $v' = 7$ and $v' = 8$, which are tiny in magnitude, and present thresholds respectively at 1.94 and 2.21 eV. Consequently, for a translational kinetic energy of 1.9 eV, pure inelastic collisions may populate excited vibrational states only up to $v = 6$. For a collision energy of 4.5 eV, we have obtained nonzero STS-SPs for inelastic excitation up to $v' = 17$.

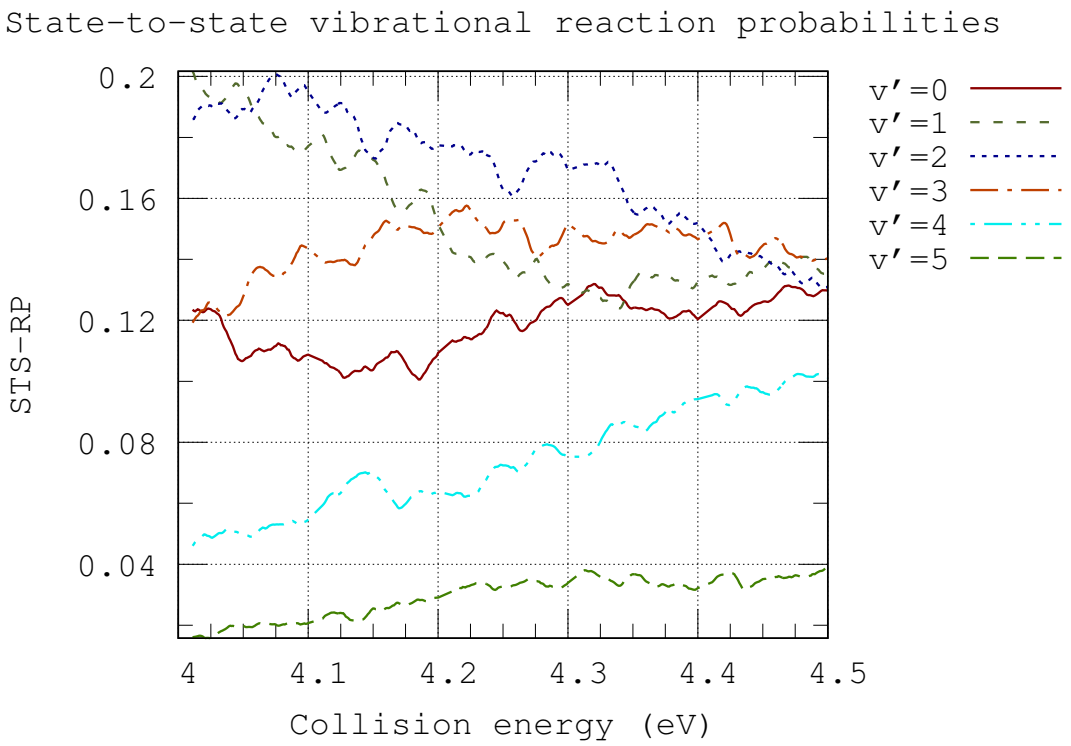

Figure 6: Vibrational state-to-state resolved reaction probabilities for atom exchange process of ^{15}N in o-^{14}N^{14}N in its ground rovibrational state: the 5 + o44($v = 0, j = 0$) $\rightarrow$ 4 + 54(v', all j') processes, as a function of collision energy in eV.

We can carry out the same kind of analysis for the STS-RPs shown in Fig. 6. For these very high collision energies, there is no clear ordering for probabilities to obtain products ^{15}N^{14}N in $v' = 0, 1, 2$ or 3. However, going to the highest collision energy of 4.5 eV, and

extrapolating toward 5.0 eV, these first four RPs seem to converge to the same value of roughly 0.14. More than that, the curve associated to $v' = 4$, initially well below the other three, seems to rise toward this value at higher energies. On the contrary, the probability to $v' = 5$, while nearly monotonic increasing with E_c, stays at values less than 0.04.

Surprisingly enough, the RP leading to products in the ground vibrational state, $v' = 0$, is not the largest. At 4.05 eV, it has half the value of that leading to products with $v' = 2$. Actually, it is significantly lower than RPs yielding the isotopologue $^{14}N^{15}N$ in $v' = 1$, $v' = 2$ and $v' = 3$, for all the energy domain $[4.0, 4.5]$ eV. As for the inelastic case, all STS-RPs to final vibrational states $v' > 17$ are found to be zero. This atom exchange reaction is quite efficient in providing significantly high vibrational levels. The translational form of kinetic energy is thus, for this system, very effective in promoting reaction products in highly excited vibrational states. These results are most relevant to the difficult problem of energy partitioning in plasma physics, in the context of spacecraft re-entry in nitrogen-rich atmospheres.[13]

To obtain converged integral cross sections and rate constants at temperatures up to 10 000 K would require supplementary calculations at total angular momentum $J > 0$, for the same collision energies. To complete these results, we plan to perform TDWP calculations for the same 5 + 44 reaction. Due to the demanding computational power, they are quite challenging for this high energy range within a full coupled-channel TIQM technique.

Conclusions

We have performed the first time-independent full quantum study of the $^{15}N + {}^{14}N^{14}N$ inelastic activation and reactive (isotope exchange) collisions starting with spin isomer ortho-$^{14}N^{14}N$, with even-j rotational states. This work is however restricted to zero total angular momentum. The dynamical calculations are supported by a recently developed full ab initio potential energy surface, the GV-DMBE PES,[25] which has already been used[28] for scattering

purposes in QCT, giving results in global good agreement with those based on other N_3 PESs. Total probabilities for this reaction have been obtained for a range of collision energies relevant to the study of the active nitrogen chemistry, initiated in shock waves resulting from the re-entry of spacecrafts in nitrogen-rich atmospheres. Numerous resonances are observed, surviving the summation over all final states, giving highly structured scattering and reaction probabilities. Collisions at energies around 2.0 eV are most effective for inelastic translation-vibration energy transfer, while those at energies close to 4.5 eV favor the atom exchange reaction, populating highly excited products rovibrational states. The intimate details of the mechanisms involved would deserve a study of its own right. We plan further study on this system, notably the influence of highly vibrationally excited $^{14}N^{14}N$ reagent on the reactivity, and the computation of dynamical observables for the counterpart collision 5 + p44.

Appendix

In absence of spin-dependent interactions in the hamiltonian describing the dynamics, the total wavefunction can be written as a direct product of three different parts, that is

$$\psi = \psi_{\text{el}}\psi_{\text{nuc.space}}\psi_{\text{nuc.spin}} \tag{1}$$

The first is the electronic (including spin) wavefunction. The ground state PES of N_3 is $^4A''$, and it is antisymmetric (but asymptotically symmetric) versus binary exchange of nuclei. The second part describes the nuclear dynamics. The third part is the nuclear spin function.

As already mentioned, ^{14}N nuclei have nuclear spin $i = 1$ and as such are bosons. As a result of the Pauli principle, the total wavefunction for the 544 system has to be symmetric with respect to the exchange of two identical ^{14}N nuclei.

The permutation group of two particles, $\mathcal{S}_2$, is also often noted C_s, with character table:

$\mathcal{S}_2(\simeq \mathrm{C}_s)$	$(1)(2) = e$ (E)	(12) (σ_v)
$\square\square$ (A')	1	1
$\begin{smallmatrix}\square\\\square\end{smallmatrix}$ (A'')	1	-1

The two IRs of the abelian $\mathcal{S}_2$ group are one-dimensional, and noted $\square\square$ or A' and $\begin{smallmatrix}\square\\\square\end{smallmatrix}$ or A''.

Let i, with projection m_i, be the spin of ^{14}N ($i = 1$) nucleus and I be the total nuclear spin of ^{14}N^{14}N with projection M_I. We can work in coupled representation and define the total spin function of 44 as:

$$\phi_{IM_I} = \sum_{m_i} C(iiI; M_I - m_i, m_i)\phi_{im_i}\phi_{iM_I - m_i} \tag{2}$$

where ϕ_{im_i} are the individual nuclei spin functions and $C(\bullet\,\bullet\,\bullet;\bullet,\bullet)$ is a Clebsch-Gordan coefficient, with resulting spin quantum numbers taking the integer values $I \in [[0, 2]]$ and $M_I = -I,\ -I+1,\ \ldots,\ +I$. It exhibits a definite parity under the transposition (12) (binary exhange of the two nuclei):

$$(12)\phi_{IM_I} = (-)^{2i-I}\phi_{IM_I} = (-)^I\phi_{IM_I} \tag{3}$$

Neglecting any spin-rotation and spin-spin couplings, the diatom wavefunction can be written:

$$\Phi = \phi_{\mathrm{el}}\phi_{vj}\phi_{IM_I} \tag{4}$$

where ϕ_{el} is the $^1\Sigma_g^+$ electronic state (of positive parity) of $^{14}\mathrm{N}_2$ and ϕ_{vj} is a rovibrational state, and thus has the parity:

$$(12)\Phi = (-)^j(-)^I\Phi = +\Phi \tag{5}$$

We can construct the following table to count nuclear spin states:

I	2	1	0
$2I+1$	5	3	1

This permits the classification of the $(2i+1)^2 = 3^2 = 9$ nuclear spin states of $^{14}N^{14}N$ between 6 ortho states o44 ($\phi_{IM_I} \in A'$, I even and j even) and 3 para states p44 ($\phi_{IM_I} \in A''$, I odd and j odd).

In the case where the atom in the entrance channel is distinguishable, i.e. ^{15}N, we would be in the presence of a process of the form:

$$5 + 44 \longrightarrow \begin{cases} 5 + 44 & (\alpha) \\ 54 + 4 & (\beta) \end{cases}$$

with inelastic (α) SPs, $P^{J\Omega}(E_c)$, expressed for $J = \Omega = 0$ as:

$$P^{00}_{\alpha\, v\, j \to \alpha\, v'\, j'}(E_c) = \begin{cases} \frac{2}{3} P^{00,A'}_{\alpha\, v\, j \to \alpha\, v'\, j'} \ [j,\, j' \text{ even}] \\ \frac{1}{3} P^{00,A''}_{\alpha\, v\, j \to \alpha\, v'\, j'} \ [j,\, j' \text{ odd}] \end{cases}$$

and with correponding reactive (β) RPs, $N^{J\Omega}(E_c)$, given by:

$$N^{00}_{\alpha\, v\, j \to \beta\, v'\, j'}(E_c) = \begin{cases} \frac{2}{3} N^{00,A'}_{\alpha\, v\, j \to \beta\, v'\, j'} \ [j \text{ even}] \\ \frac{1}{3} N^{00,A''}_{\alpha\, v\, j \to \beta\, v'\, j'} \ [j \text{ odd}] \end{cases}$$

Acknowledgement

TIQM calculations were performed using HPC resources from DSI-CCUB (Université de Bourgogne). The authors thank Antonio Varandas for sending them the N_3 potential energy surface.

References

(1) Clayton, D. D. ^{22}Na, Ne–E, extinct radioactive anomalies and unsupported ^{40}Ar. *Nature* **1975**, *257*, 36–37.

(2) Fallick, A. E.; Pillinger, C. T. The third category of extraterrestrial material. *Nature* **1980**, *285*, 10–11.

(3) Kerridge, J. F. Whence so much ^{15}N ? *Nature* **1982**, *295*, 643–644.

(4) Marty, B.; Zimmermann, L.; Burnard, P. G.; Wieler, R.; Heber, V. S.; Burnett, D. L.; Wiens, R. C.; Bochsler, P. Nitrogen isotopes in the recent solar wind from the analysis of Genesis targets: Evidence for large scale isotope heterogeneity in the early solar system. *Geochimica et Cosmochimica Acta* **2010**, *74*, 340–335.

(5) Marty, B.; Chaussidon, M.; Wiens, R. C.; Jurewicz, A. J. G.; Burnett, D. S. A ^{15}N-Poor Isotopic Composition for the Solar System As Shown by Genesis Solar Wind Samples. *Science* **2011**, *332*, 1533–1536.

(6) Yeung, L. Y.; Li, S.; Kohl, I. E.; Haslun, J. A.; Ostrom, N. E.; Hu, H.; Fischer, T. P.; Schauble, E. A.; Young, E. D. Extreme enrichment in atmospheric ^{15}N^{15}N. *Science Advances* **2017**, *3*, eaao6741.

(7) Gelfand, N.; Komarova, K.; Remacle, F.; Levine, R. D. On the Energy-specific Photodissociation Pathways of $^{14}N_2$ and ^{14}N^{15}N Isotopomers to N Atoms of Different Reactivity: A Quantum Dynamical Perspective. *Astrophys. J.* **2023**, *948*, 58.

(8) Back, R. A.; Mui, J. Y. P. The reactions of active nitrogen with ^{15}NO and $^{15}N_2$. *J. Phys. Chem.* **1962**, *66*, 1362–1364.

(9) Bauer, S. H.; Tsang, S. C. Mechanisms for Vibrational Relaxation at High Temperatures. *Phys. Fluids* **1963**, *6*, 182–189.

(10) Lyon, R. K. Search for the N – N_2 Exchange Reaction. *Can. J. Chem.* **1972**, *50*, 1437–1440.

(11) Bar-Nun, A.; Lifshitz, A. Kinetics of the Homogeneous Exchange Reaction: $^{14-14}N_2$ + $^{15-15}N_2 \rightarrow 2\ ^{14-15}N_2$. Single-Pulse Shock-Tube Studies. *J. Chem. Phys.* **1967**, *47*, 2878–2888.

(12) Morgan, J. E.; Schiff, H. I. The Study of Vibrationally Excited N_2 Molecules with the Aid of an Isothermal Calorimeter. *Can. J. Chem.* **1963**, *41*, 903–912.

(13) Zhu, T.; Li, Z.; Levin, D. A. Development of a two-dimensional binning model for N_2 – N relaxation in hypersonic shock conditions. *J. Chem. Phys.* **2016**, *145*, 6.

(14) Laganà, A.; Garcia, E.; Ciccarelli, L. Deactivation of vibrationally excited nitrogen molecules by collision with nitrogen atoms. *J. Phys. Chem.* **1987**, *91*, 312–314.

(15) Garcia, E.; Laganà, A. The largest angle generalization of the rotating bond order potential: The H + H_2 and N + N_2 reactions. *J. Chem. Phys.* **1995**, *103*, 5410–5416.

(16) Garcia, E.; Laganà, A. Effect of Varying the Transition State Geometry on N + N_2 Vibrational Deexcitation Rate Coefficients. *J. Phys. Chem. A* **1997**, *101*, 4734–474.

(17) Garcia, E.; Saracibar, A.; Gómez-Carrasco, S.; Laganà, A. Modeling the global potential energy surface of the N + N_2 reaction from ab initio data. *Phys. Chem. Chem. Phys.* **2008**, *10*, 2552–2558.

(18) Rampino, S.; Skouteris, D.; Laganà, A.; Garcia, E.; Saracibar, A. A comparison of the quantum state-specific efficiency of N + N_2 reaction computed on different potential energy surfaces. *Phys. Chem. Chem. Phys.* **2009**, *11*, 1752–1757.

(19) Petrongolo, C. MRD-CI quartet potential surfaces for the collinear reactions $N(^4S_u)$+$N_2(X^1\Sigma_g^+$, $A^3\Sigma_u^+$, and $B^3\Pi_g)$. *J. Mol. Struct.* **1989**, *202*, 135–142.

(20) Wang, D.; Stallcop, J. R.; Huo, W. M.; Dateo, C. E.; Schwenke, D. W.; Partridge, H. Quantal study of the exchange reaction for N + N_2 using an ab initio potential energy surface. *J. Chem. Phys.* **2003**, *118*, 2186–2189.

(21) Wang, D.; Huo, W. M.; Dateo, C. E.; Schwenke, D. W.; Stallcop, J. R. Reactive resonances in the N + N_2 exchange reaction. *Chem. Phys. Lett.* **2003**, *379*, 132–138.

(22) Wang, D.; Huo, W. M.; Dateo, C. E.; Schwenke, D. W.; Stallcop, J. R. Quantum study of the N + N_2 exchange reaction: State-to-state reaction probabilities, initial state selected probabilities, Feshbach resonances, and product distributions. *J. Chem. Phys.* **2004**, *120*, 6041–6050.

(23) Wang, Y.; Meng, F.; Yan, P.; Wang, D. Quantum dynamics study of energy efficiency on reactivity for the double-barrier potential energy surface of the N + N_2 reaction. *Chem. Phys. Lett.* **2015**, *633*, 202–207.

(24) Stallcop, J. R.; Partridge, H.; Levin, E. Effective potential energies and transport cross sections for atom-molecule interactions of nitrogen and oxygen. *Phys. Rev. A* **2001**, *64*, 042722.

(25) Galvão, B. R. L.; Varandas, A. J. C. Accurate Double Many-Body Expansion Potential Energy Surface for $N_3(^4A'')$ from Correlation Scaled ab Initio Energies with Extrapolation to the Complete Basis Set Limit. *J. Phys. Chem. A* **2009**, *113*, 14424–14430.

(26) Faginas, N.; Huarte-Larrañaga, F.; Laganà, A. Full dimensional quantum versus semiclassical reactivity for the bent transition state reaction N + N_2. *Chem. Phys. Lett.* **2008**, *464*, 249–255.

(27) Skouteris, D.; Castillo, J.; Manolopoulos, D. ABC: a quantum reactive scattering program. *Comp. Phys. Com.* **2000**, *133*, 128–135.

(28) Caridade, P. J. S. B.; Galvão, B. R. L.; Varandas, A. J. C. Quasiclassical Trajectory Study of Atom-Exchange and Vibrational Relaxation Processes in Collisions of Atomic and Molecular Nitrogen. *J. Phys. Chem. A* **2010**, *114*, 6063–6070.

(29) Launay, J. M.; Dourneuf, M. L. Hyperspherical Close-Coupling Calculation of Integral Cross Sections for the Reaction H + H_2 - H_2 + H. *Chem. Phys. Lett.* **1989**, *163*, 178–188.

(30) Rao, T. R.; Guillon, G.; Mahapatra, S.; Honvault, P. Huge Quantum Symmetry Effect in the O + O_2 Exchange Reaction. *J. Phys. Chem. Lett.* **2015**, *6*, 633–636.

(31) Guillon, G.; Honvault, P.; Kochanov, R.; Tyuterev, V. First-Principles Computed Rate Constant for the O + O_2 Isotopic Exchange Reaction Now Matches Experiment. *J. Phys. Chem. Lett.* **2018**, *9*, 1931–1936.

(32) Guillon, G.; Honvault, P. Quantum Dynamics of the ^{17}O + $^{32}O_2$ Collision Process. *J. Phys. Chem. A* **2016**, *120*, 8254–8258.

(33) Guillon, G.; Honvault, P. Quantum dynamics of ^{16}O in collision with ortho- and para-$^{17}O^{17}O$. *Chem. Phys. Lett.* **2017**, *689*, 62–67.

(34) Guillon, G.; Lepers, M.; Honvault, P. Quantum dynamics of ^{17}O in collision with ortho- and para-$^{17}O^{17}O$. *Phys. Rev. A* **2020**, *102*, 012810.

(35) Delves, L. M. Tertiary and general-order collisions. *Nature Physics* **1958**, *9*, 391–399.

(36) Whitten, R. C.; Smith, F. T. Symmetric Representation for Three-Body Problems. II. Motion in Space. **1968**, *9*, 1103–1113.

(37) Smith, F. T. Generalized Angular Momentum in Many-Body Collisions. *Phys. Rev.* **1960**, *120*, 1058–1069.

(38) Johnson, B. R. The Multichannel Log-Derivative Method for Scattering Calculations. *J. Comp. Phys.* **1973**, *13*, 445–449.

(39) Manolopoulos, D. E. An Improved Log-Derivative Method for Inelastic Scattering. *J. Chem. Phys.* **1986**, *85*, 6425–6429.

(40) Lepetit, B.; Launay, J. M. A Quantum-Mechanical Study of the Reaction H + HF$(v, j, m_j) \rightarrow$ HF(v', j', m'_j) + H: Exact and Centrifugal Decoupling Calculations in Hyperspherical Coordinates. *Chem. Phys. Lett.* **1988**, *151*, 287–295.

(41) Miller, W. H.; Schwartz, S. D.; Tromp, J. W. Quantum mechanical rate constants for bimolecular reactions. *J. Chem. Phys.* **1983**, *79*, 4889–4898.

TOC Graphic

Some journals require a graphical entry for the Table of Contents. This should be laid out "print ready" so that the sizing of the text is correct.
Inside the `tocentry` environment, the font used is Helvetica 8 pt, as required by *Journal of the American Chemical Society*.
The surrounding frame is 9 cm by 3.5 cm, which is the maximum permitted for *Journal of the American Chemical Society* graphical table of content entries. The box will not resize if the content is too big: instead it will overflow the edge of the box.
This box and the associated title will always be printed on a separate page at the end of the document.